Advances in Nano Research, *Vol. 12, No. 5 (2022) 501-514*
https://doi.org/10.12989/anr.2022.12.5.501

Effects of exploration and molecular mechanism of CsV on eNOS and vascular endothelial functions

Deyu Zuo[1], Heng Jiang[1], Shixiong Yi[1], Yang Fu[1], Lei Xie[1], Qifeng Peng[1], Pei Liu[1], Jie Zhou*[1] and Xunjia Li**[2]

[1]*Department of Rehabilitation Medicine*, *Chongqing Traditional Chinese Medicine Hospital*, *Chongqing*, *China*
[2]*Department of Nephrology*, *Chongqing Traditional Chinese Medicine Hospital*, *Chongqing*, *China*

(*Received January 27, 2022, Revised March 4, 2022, Accepted March 6, 2022*)

Abstract. This study aimed to investigate the effects and potential mechanisms of Chikusetsusaponin V (CsV) on endothelial nitric oxide synthase (eNOS) and vascular endothelial cell functions. Different concentrations of CsV were added to animal models, bovine aorta endothelial cells (BAECs) and human umbilical vein endothelial cells (HUVECs) cultured in vitro. qPCR, Western blotting (WB), and B ultrasound were performed to explore the effects of CsV on mouse endothelial cell functions, vascular stiffness and cellular eNOS mRNA, protein expression and NO release. Bioinformatics analysis, network pharmacology, molecular docking and protein mass spectrometry analysis were conducted to jointly predict the upstream transcription factors of eNOS. Furthermore, pulldown and ChIP and dual luciferase assays were employed for subsequent verification. At the presence or absence of CsV stimulation, either overexpression or knockdown of purine rich element binding protein A (PURA) was conducted, and PCR assay was employed to detect PURA and eNOS mRNA expressions, Western blot was used to detect PURA and eNOS protein expressions, cell NO release and serum NO levels. Tube formation experiment was conducted to detect the tube forming capability of HUVECs cells. The animal vasodilation function test detected the vasodilation functions. Ultrasonic detection was performed to determine the mouse aortic arch pulse wave velocity to identify aortic stiffness. CsV stimulus on bovine aortic cells revealed that CsV could upregulate eNOS protein levels in vascular endothelial cells in a concentration and time dependent manner. The expression levels of eNOS mRNA and phosphorylation sites Ser1177, Ser633 and Thr495 increased significantly after CsV stimulation. Meanwhile, CsV could also enhance the tube forming capability of HUVECs cells. Following the mice were gavaged using CsV, the eNOS protein level of mouse aortic endothelial cells was upregulated in a concentration- and time-dependent manner, and serum NO release and vasodilation ability were simultaneously elevated whereas arterial stiffness was alleviated. The pulldown, ChIP and dual luciferase assays demonstrated that PURA could bind to the eNOS promoter and facilitate the transcription of eNOS. Under the conditions of presence or absence of CsV stimulation, overexpression or knockdown of PURA indicated that the effect of CsV on vascular endothelial function and eNOS was weakened following PURA gene silence, whereas overexpression of PURA gene could enhance the effect of CsV upregulating eNOS expression. CsV could promote NO release from endothelial cells by upregulating the expression of PURA/eNOS pathway, improve endothelial cell functions, enhance vasodilation capability, and alleviate vessel stiffness. The present study plays a role in offering a theoretical basis for the development and application of CsV in vascular function improvement, and it also provides a more comprehensive understanding of the pharmacodynamics of CsV.
Keywords: cardiovascular disease; CsV; endothelial cell function; eNOS; PURA

1. Introduction

In the last decade, improved material responses and advantages in sciences and technology made many opportunities in medical issues. Accordingly, vascular endothelial cells manifest multiple vital biological activities and characterized by active endocrine functions, allowing to sense physiological stimuli and regulate responses to maintain the balance of the endovascular environment. Endothelial functions include endothelium-dependent stimulations, namely changes in blood flow shear stress, ischemia and certain drugs. The endothelium produces vasoactive substances through its ability to react accordingly, and regulates the normal systolic and diastolic responses of the coronary arteries to maintain blood fluidity (Vanhoutte *et al*. 2017). The functions of endothelial cells can be impaired due to ischemia, lipid deposition, and mechanical damage to hemodynamics as a result of endothelial dysfunction. And are closely correlated with several cardiovascular diseases like atherosclerosis, hypertension, and unstable angina. Risk factors of cardiovascular disease initially act on endothelial cells, leading to endothelial dysfunction, and endothelial function damage and aggravates cardiovascular diseases (Godo and Shimokawa 2017).

Endothelial nitric oxide synthase (eNOS) refers to the nitric oxide synthase (NOS) that mainly exists in endothelial cells, serving as a key enzyme involved in regulating diastolic function of the cardiovascular system.

*Corresponding author, Chief physician,
E-mail: cqszyyzj@163.com
**Co-corresponding author, Ph.D.,
E-mail: cqlixunjia@163.com

ISSN: 2287-237X (Print), 2287-2388 (Online)

The cells are recognized as one of the most important endogenous vasodilator factors (Tsutsui *et al*. 2009). The NO produced by eNOS catalyzed by L-arginine can regulate vascular tension, inhibit the proliferation of vascular smooth muscle cells, mediate vascular endothelial-dependent angiogenesis and thrombosis, so as to maintain the homeostasis of the cardiovascular system (Boucher *et al*. 1999). NO released by endothelial cells in the basal state participates in maintaining the normal tension of blood vessels, which is of great significance to the protection of endothelial function.

Panax japonicus is a species included in the Pharmacopoeia of the People's Republic of China. It is clearly identified as the dried rhizome of *Panax japonicus C. A. Mey*, and is effective in invigorating deficiency and reinforcing strength, suppressing cough and eliminating phlegm, dispelling blood stasis and hemostasis, detumescence and relieving pain. The main ingredient of *Panax japonicus* is Chikusetsusaponin, of which the content of Chikusetsusaponin V (CsV) is the highest and it is one of the most effective ingredients. Previous studies have found that Chikusetsusaponin can protect the cardiovascular vessels. Animal experiments have proved that *Panax japonicus* extract can enhance the amplitude of animal's cardiac contractions, cardiac output and coronary blood flow, upregulate the ratio of cAMP/cGMP in the myocardium, and strengthen the heart and benefit blood vessel dilation. In vitro experiments have indicated that Chikusetsusaponin IVa can improve the survival rate of cardiomyocytes in myocardial injury model (Huang *et al*. 2021b, c, Ma *et al*. 2021, Zhao *et al*. 2021, Yu *et al*. 2022). Additional experiments have shown that the total saponins of *Panax japonicus* can exert satisfactory protective effects on cerebral ischemia injury, and substantially inhibit the NOS activity in the hippocampus of animals with cerebral ischemia injury. However, few researches have been carried out to explore the effect of CsV on vascular endothelial function and eNOS.

Previous studies have revealed that CsV can upregulate eNOS protein levels in vascular endothelial cells in a concentration and time dependent manner. The mRNA expression level of eNOS and the phosphorylation sites Ser1177, Ser633 and Thr495 all increased markedly after CsV stimulation. In addition, some studies have also reported that CsV can enhance the tube formation ability of HUVECs cells. It is therefore that we put forward the hypothesis: CsV can monitor vascular endothelial function by regulating the expression of eNOS.

2. Materials and methods

2.1 Cell culture

Both BAECs and HUVECs were purchased from ATCC (USA). BAECs were cultured in vitro with DMEM medium containing 100 U/mL penicillin, 100 mg/mL streptomycin and 10% FBS, Meanwhile, HUVECs were cultured using 199 medium containing 20% FBS, 20 μg/mL endothelial cell growth supplement, 100 μg/mL heparin, 2 mM L-glutamine, 1% penicillin and streptomycin. Both cell types were incubated under 5% CO2, 37°C and 95% humidity. The BAECs employed in the experiments passed 6-10 passages. The CsV stimulation on BAECs and HUVECs was performed in two approaches. One was conducted by adding CsV at different concentrations (0, 12.5, 25, 50, and 100 μM) to the culture medium of cells and lasted 24 h. The other method was to add 100 μM CsV to the culture medium at different time points (0, 6, 12, 18, and 24 h) after the culture started.

2.2 Animal feeding

The experimental animals were male C57 BL/6 mice (6-8 weeks weighing 20-25 g), which were purchased from Ensiweier Biotechnology Co., Ltd. (Chongqing, China). All mice were fed free with water and food and raised under standard conditions with 12-h light and dark alternation, the temperature was set at 23 ± 1°C, and humidity was 55 ± 5%. After weighed and randomly grouped, the animals were administered at different concentrations of CsV (0, 200, 400, 600, and 800 mg/kg) intragastrically once per day. The mice were sacrificed 28 d after injection for tissue extraction. The normal control group was given phosphate buffered saline (PBS). The administration of 800 mg/kg CsV was given by gavage at different time (0, 7, 14, 21, and 28 d, once per day).

2.3 Preparation of CsV solution

Panax japonicus decoction pieces (produced by Xinkang Pharmaceutical) were taken, added water for distillation with reflux extraction twice, and mixed the extracting solution. After pressure reduction, the obtained decoction was concentrated to an appropriate volume, subpackaged, and stored in a refrigerator. A 1000 μg/mL CsV solution was prepared by adding 10 mg CsV into 10 mL high-glucose DMEM containing 1% FBS and sterilized by using 0.22 μm filter membrane. High-glucose DMEM was used to obtain the desired concentration.

2.4 qRT-PCR

Detection of mRNA expression in the sample was carried out according to the instructions of the TAKARA kit. The reaction system was RNA, 2.2 μL, OligodT, 2 μL, dNTP, 4 μL, 5×buffer, 4 μL, Reverse Transcriptase, 1 μL, RNAase inhibitor, 0.5 μL, and RNAase free ddH2O was added to 20 μL. The reaction conditions were set at 25°C for 5 min, 50°C for 15 min, 85°C for 5 min, and 4°C for 10 min. The qRT-PCR assay was carried out in accordance with qRT-PCR kit from Tsingke Biological Technology. The reaction system was 4 μL cDNA, Forward primer, 0.4 μL, Reverse primer, 0.4 μL, SYBRGreen, 10 μL, and H2O, 5.2 μL. The reaction conditions were 50℃ for 2 min, 95℃ 10 min, 95℃ 30 sec, and 60℃ 30 sec for 40 cycles. The $2^{-\Delta\Delta CT}$ algorithm was used to calculate the relative gene expression levels.

2.5 Western blotting

The tissue were added with lysate, lysed on ice 30 min, centrifuged at 13 000 g for 15 min and the supernatant was obtained. Following the protein concentration was

determined by BCA method, the solution was diluted with loading buffer and boiled for 5 min at 100℃. The protein was separated in 10% SDS-polyacrylamide gel by electrophoresis at 80 V for 2 h, and subsequently transferred to a PVDF membrane. The membrane was blocked with 5% skimmed milk for 1 h at room temperature (RM), and incubated with the following antibodies at 4℃ overnight respectively: anti-eNOS (Cat No. 07–520), P-eNOS Ser1177 (Cat No. 07–428), P-eNOS Ser633 (Cat No. 07–562), and P-eNOS Thr495 (Cat No. 04–811) were purchased from Millipore (Massachusetts, USA). Anti-β-actin (1:1000, Beyotime) was employed as internal reference. The membrane was then washed with TBST three times, 10 min each time. Secondary antibodies (HRP Goat Anti-Rabbit IgG, 1:1 000, ABclonal) were added and incubated at RM for 1 h. The membrane was washed with TBST three times again, 10 min each time. ECL reaction solution was added, Bio-Rad developer was used for development. The Image Lab software was employed for quantitative analysis of the bands.

2.6 Cell NO release determination by the nitrate reductase method

The culture medium of each group was collected, heated in boiling water for 5 min to denature the protein, and centrifuged at 12 000 g for 5 min. The supernatant was obtained for subsequent determination. The complete medium was applied to dilute the 1M NaNO2 into 2, 5, 10, 20, 40, 60, and 80 μmol/L to prepare a standard culture solution. Approximate 3 mL of double-distilled water was supplemented to 5 mg NADPH, mixed reversely to dissolve it completely to prepare 2 mM NADPH. FAD was prepared in an appropriate solution. Nitrate Reductase and LDH were taken out and placed on ice together with other reagents for use. A 96-well plate was firstly wrapped with aluminum foil to avoid light, and then added the standard, sample, and detection reagents in sequence. Wells of negative control were supplemented with 200 μL PBS. A microplate reader at A450 wavelength was employed for the determination and a standard curve was plotted. The concentration of nitric oxide in the sample was calculated according to the standard curve.

2.7 Tube formation assay

BD Materiel (5 mg/mL, BD Biosciences, USA) was spread on a 48-well plate (120 μL/well) cushioned by ice cubes, and solidified at 37°C for 2 h. After the matrigel was solidified, HUVECs were carefully added at 3.0×10^4/well, and incubated 6 h at 37°C, 5% CO_2 incubator. The EVOS FL automatic microscopic imaging system was used and microscopic fields were randomly selected. Subsequently, Image J was applied for data analysis. Five low magnified visual fields (40×) in each well were randomly selected and the total length of the tubules and branch was calculated.

2.8 Pull down assay

The 6×His-NPM1 (pET-28a) plasmid was transformed into BL21-DE3 competent cells and cultured to induce protein expression. The 6×His-NPM1 monoclonal colonies were supplemented to 5 mL medium (containing amp antibiotics), incubated at 37°C on a shaker for 12-15 h, inoculated at 1:100 rate in 50 mL medium (containing amp antibiotics), and cultured at 37°C until the A600 absorbance value was at 0.6-0.8. By addition of 100 mM IPTG, a final concentration was set at 1.0 mM to induce expression. The culture continued at 30℃ for 2-4 h. Then the bacterial solution was centrifuged at 7700 g for 10 min. The supernatant was discarded, and the cells were dried on ice. The precipitate was resuspended using 2.5 mL PBS, and 10 μL for subsequent SDS-PAGE analysis. Next, the cells were lysed by adding 25 μL lysozyme. Dry ice to freeze and thaw three times. Ultrasound was performed for the clear bacteria solution. The supernatant was obtained by centrifuged at 12 000 g for 15 min. Glutathione sepharose 4B beads were prepared and combined with GST fusion protein. 20 μL prepared Sepharose 4B beads was taken per sample, added with 1 mL binding buffer, and then 5 μg purified GST control protein, containing six mutant proteins (1-5883aa full-length GST-PES1 protein, 1-415aa, 322-455aa deletion, 322-588aa, 220-588aa, and 101-588aa). The mixture was incubated at RM for 1 h to perform the pull-down experiment. 100 μL of His-NMP1 induced expression lysate was added to each sample, mixed overnight at 4°C, centrifuged at 500 g for 5 min and discard supernatant. Followed by 3-4 cycles of washing using lysis buffer, the samples were added with 2x SDS loading buffer and boiled for 10 min. Western blot was used to analyze the results. Antibodies were detected using anti-HIS labels.

2.9 Mass spectrometry analysis

Mass spectrometry was performed by BestNovo (Beijing) Medical Technology Co., Ltd.

2.10 Molecular docking

AutoDock and MATLAB softwares (Liu *et al*. 2020a, b, Zhou *et al*. 2020, Dai *et al*. 2021a, Habibi *et al*. 2021, Hou *et al*. 2021, Huang *et al*. 2021a, b, d, Jiao *et al*. 2021, Liu *et al*. 2021, Moradi *et al*. 2021, Shao *et al*. 2021, Wu and Habibi 2021, Xu *et al*. 2021, Zhang *et al*. 2021, Dong *et al*. 2022, Luo *et al*. 2022, Yang *et al*. 2022, Yu *et al*. 2022) was employed to perform molecular docking described as described previously. The binding preference of CsV on PURA was analyzed.

2.11 Chromatin immunoprecipitation assay (ChIP)

After the cells grew to 80%~90%, the supernatant was removed and 37% formaldehyde (final concentration 1%) was added to fix the cross-linked cells. Ten min later, 0.125 mol/L glycine was added to terminate the crosslinking at RM for 5 min. The cells were collected with a scraper and cell lysate was added and genomic DNA was extracted according to the instructions of genomic DNA extraction kit. The DNA was broken into length of 200-1000 bp using an ultrasonic cell crusher. 20 μL Protein A/G Agarose Beads were added, and gently shaken at 4℃ for 1 h to remove non-specific antibody. The immunoprecipitation antibody was added to the supernatant, vibrated mildly at 4℃ overnight, and the immune complex (antibody-protein-

DNA) was harvested. In addition, 50 μL supernatant free of antibody addition was taken as negative control to verify the detection characteristics. The beads were washed by being added with 200 μL ChIP elution solution with three repeats to obtain 600 μL eluent. As the eluent contained protein of interest and associated binding DNA, by supplementing 24 μL 5 mol/L NaCI, formaldehyde crosslinking was removed overnight. Anhydrous ethanol was provided and placed at -80℃ for 45 min, the cells were washed using 70% ethanol twice, added TE buffer (10 mM Tris-HCl, 1mM EDTA, pH8.0) to dissolve the precipitation, and supplemented with 50 μg protease K and bathed at 50℃ for 30 min. Equal volume of phenol/chloroform/ isopentyl alcohol (25:24:1) was added for extraction twice and the supernatant was collected. 2 μL glycogen and 2 times volume of anhydrous ethanol were added, placed at -20℃ for 2 h, and centrifuged. The precipitate was washed with anhydrous ethanol once, and the IP DNA precipitate was resuspended with 30-50 μL sterilized water. Chromatin immunoprecipitation DNA was analyzed and protein binding sites on DNA were identified. Primers were designed based on the target sequences. Quantitative fluorescence PCR was used to compare the amount of DNA products precipitated by specific and non-specific immunoantibodies.

2.12 Dual-luciferase assay

Cell and plasmid transfection were grouped as follows: NC+peNOS-promoter-WT, NC+peNOS-promoter-mut, pCMV-PURA+peNOS-promoter-WT, and pCMV-PURA+ peNOS-promoter-mut. Luciferase Assay Reagent II (LAR II) working solution was added to the 96-well plate, mixed with cell lysate, to determine and record the Firefly luciferase value, which was used as the luminescence value of the reporter gene. After adding 100 μL Stop & Glo® Reagent the Rinella luciferase values were measured and recorded, which was used as the internal reference value.

2.13 Vasodilation function determination

C57 BL/6 mice were anesthetized using sodium pentobarbital (3.5 mg/100 g), The thoracic aorta of the mice was isolated immediately, the adhering lipid and connective tissue were dissociated, and was cut into vascular rings of 2-3 mm in width, Then immersed in bicarbonate buffer (NaCl: 130 μmol/L, NaHCO3: 14.9 μmol/L, KCl: 4.7 μmol/L, KH2PO4: 1.18 μmol/L, MgSO4: 1.17 μmol/L, CaCI2: 1.6 μmol/L, Ethylenediaminetetraacetic acid (EDTA): 0.026 μmol/L, glucose: 5.5 μmol/L, physiological aqueous solution (PSS) of PH value at 7), And fixed on a Mulvany-Halpern myograph (620M, DMT, Denmark), the test was started after equilibration for 60 min, The DMT transducer system was preloaded with the vascular rings and collected the tension data and input in the computer applying LabChart software, After equilibration, the samples were stimulated using potassium-physiological salt solution (K-PSS) containing bicarbonate buffer for 10 min, Then, the vascular rings were washed with PSS, Norepinephrine (NE) solution (10^{-7} mol/L, the First Affiliated Hospital-Chongqing medical university) was employed to stimulate. Ultimately, the cumulative concentration effect curve of thoracic aorta was plotted which was under the action of endothelium-dependent relaxation agonist-acetylcholine (ACh, 10^{-8}-$10^{-5.5}$ mol/L, Sangon Biotech (Shanghai) Co., Ltd.).

2.14 Ultrasound detection of mouse aortic arch pulse wave velocity (PWV)

After anesthesia, the mice were fixed in a supine position, and the skin of anterior thorax was fully prepared and underwent detection using echocardiographic Doppler (Vevo3100, VisualSonics Inc., Toronto, ON, Canada). The displacement distance along the arch of the aorta between both points was measured on the same imaging plane, which was defined as D1. Combined with ECG monitoring, the time difference between QRS wave in ascending aorta (aortic ring) and Doppler wave in ascending aorta was recorded as T1, The time difference between QRS wave of the descending aorta and Doppler wave of the descending aorta was recorded as T2 (T1 and T2 records were not less than 10 consecutive cardiac cycles). The formula of mouse aortic arch pulse wave velocity was calculated as PWV = D1/[T2 - T1 (cm/s)].

2.15 Function recovery verification test

The eNOS-binding protein screened in the previous experiment was used by silencing and overexpressing at the cellular and animal level respectively, and the endothelial cells and vascular functions were observed with or without CsV stimulus. Non-CSV stimulus grouping: silent control group, silent group, overexpression control group, and overexpression group. CSV stimulus grouping: control group, CsV group, silent group, CsV+ silent group, overexpression group, and CsV+overexpression group. The mRNA and protein expression of eNOS were determined, and the amount of cell NO release and serum NO level were detected. Tubule formation assay was used to measure the tubule formation ability, vasodilation function and aorta stiffness of HUVECs cells.

2.16 Statistical analysis

Graphpad 6.0 software was used (Habibi *et al*. 2019b), and the test data were expressed as mean ± SD (standard deviation) (Adamian *et al*. 2020, Bai *et al*. 2020, Li *et al*. 2020a, b, Zare *et al*. 2020, Zhang *et al*. 2020, Dai *et al*. 2021b, Guo *et al*. 2021). One-way ANOVA test was employed for statistical analysis among groups. $P < 0.05$ was considered statistically significant (Habibi *et al*. 2019a, Ebrahimi *et al*. 2020, Chen *et al*. 2022).

3. Results

3.1 Effects of CsV on intracellular eNOS expression and endothelial functions

We treated BAECs with 0, 12.5, 25, 50, and 100 μM of CsV for 24 h, and detected the expression of eNOS protein by WB. The results were shown in Figs. 1A and 1B, the expression of eNOS increased with the increased concentration of CsV ($p < 0.05$), The amount of cell NO

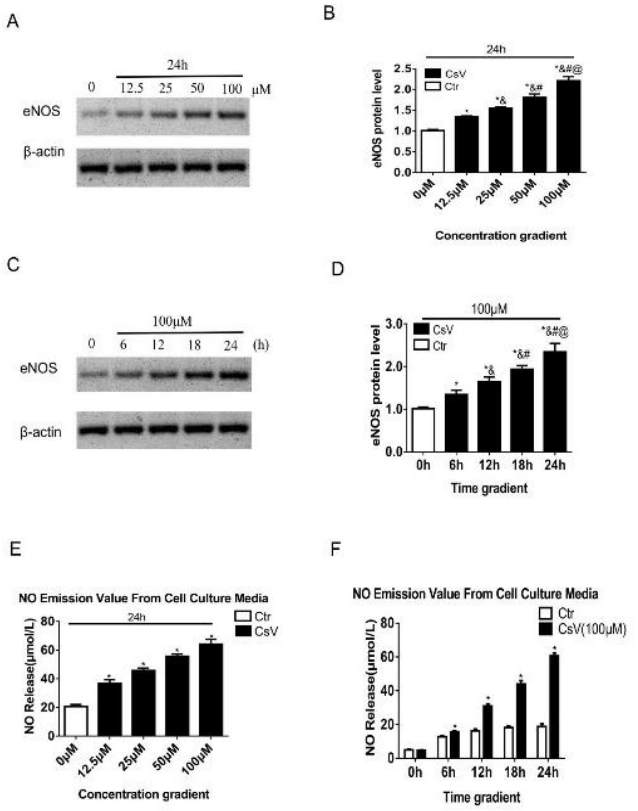

Fig. 1 Effects of CsV on intracellular eNOS expression and endothelial functions

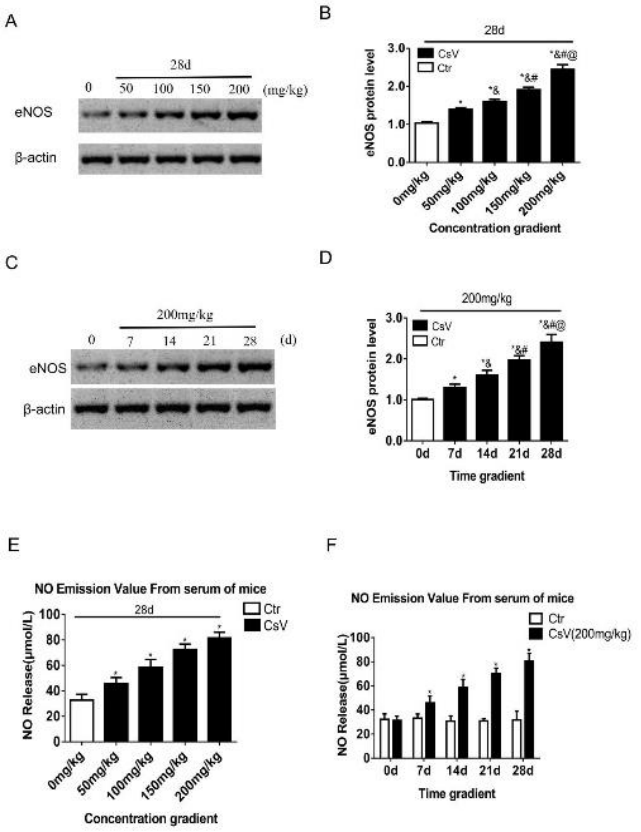

Fig. 3 Effects of CsV on eNOS and vasodilation in mice

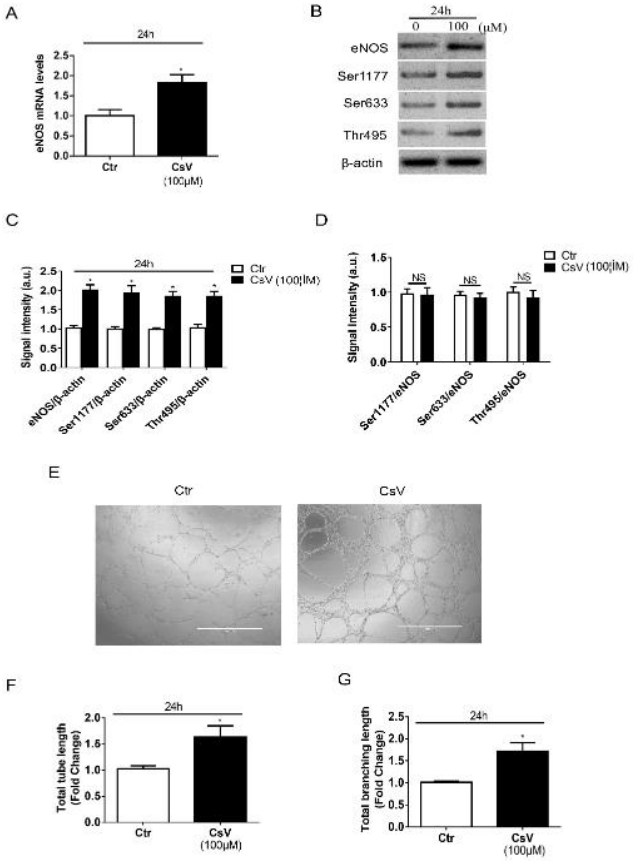

Fig. 2 Effects of CsV on tube formation capability, eNOS and vasodilation function in mice

release was detected as shown in Fig. 1E, and the amount of NO released also increased with the increase of CsV concentration ($p < 0.05$). We subsequently selected 100 μM CsV for BAECs treatment 0, 6, 12, 18, and 24 h, and detected the expression of eNOS protein using WB. The results were presented in Fig. 1C-D, the expression level of eNOS increased with the increase of CsV treatment time ($p < 0.05$), The cell NO release was detected as shown in Fig. 1F, and the NO release also increased with the increase of CsV treatment time ($p < 0.05$). According to the described experimental results, the optimal concentration (100 μM) and optimal time (24 h) of CsV were selected to treat BAECs. RT-qPCR was used to detect the expression of eNOS mRNA (Fig. 2A) and the results showed that the expression of eNOS after CsV treatment was markedly higher than that of the control group ($p < 0.05$). WB detection was conducted to determine the protein expression of total eNOS and its phosphorylation sites. The results were shown in Fig. 2B-C. After CsV treatment, the protein expressions of total eNOS and its phosphorylation sites were markedly elevated compared with the control group ($p < 0.05$). Further comparison of the protein expression levels of eNOS phosphorylation sites Ser1177, Ser633, and Thr495 and total eNOS indicated no statistical significance (Fig. 2D), suggesting that an increase in total eNOS protein content resulted in an increase in protein content at the corresponding phosphorylation site.

The tubule formation assay was used to detect the tube formation ability of HUVECs. The results were shown in Figs. 2E-2G. The total tubule length and total branch length of HUVECs increased following the treatment with 100 μM

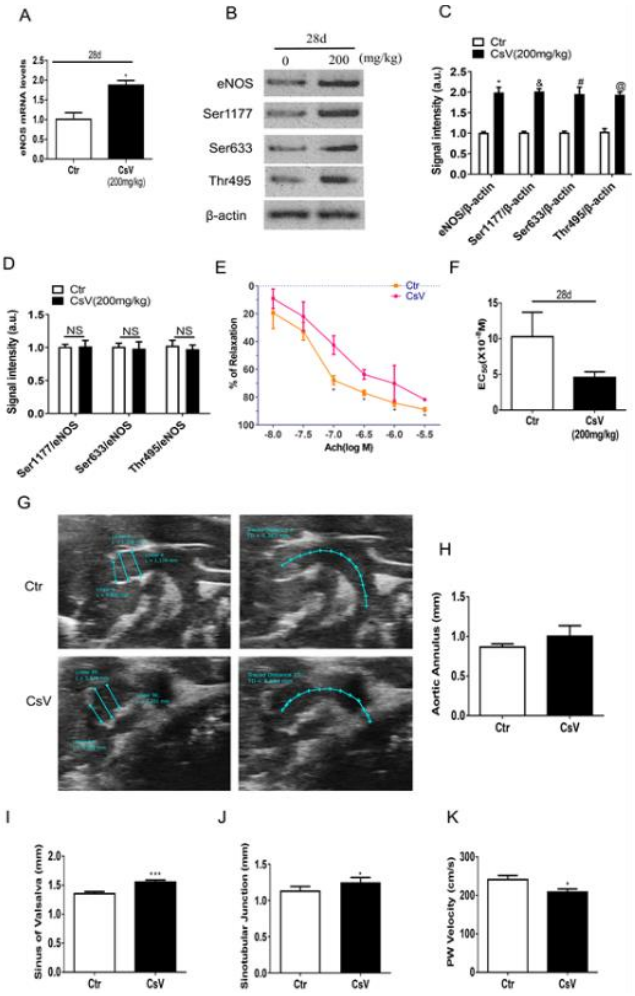

Fig. 4 Effects of CsV on vasodilation and vascular stiffness in mice

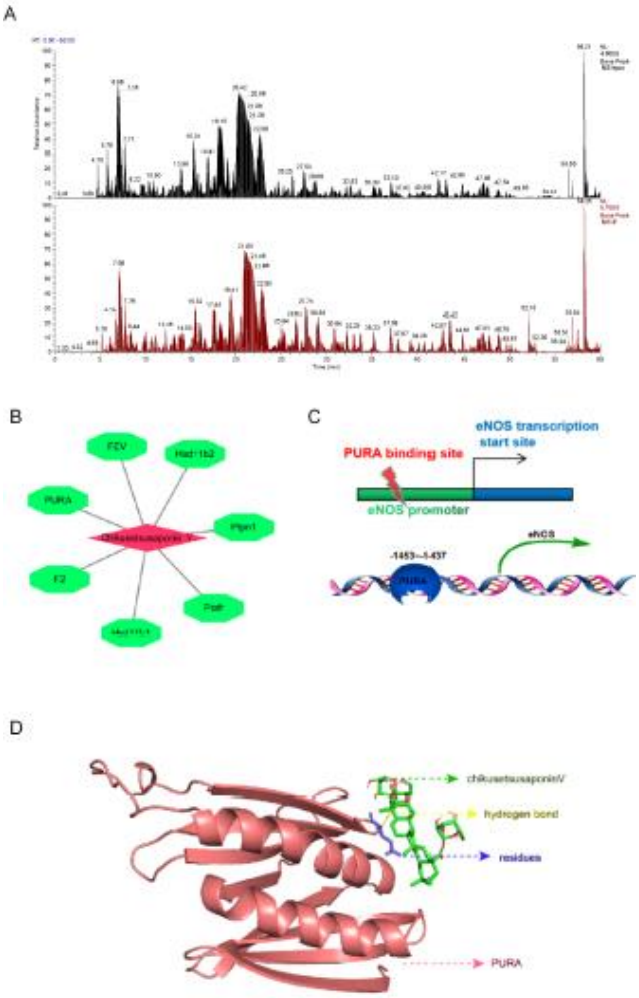

Fig. 5 Prediction and screening of eNOS upstream transcription factors

CsV for 24 h compared with the control group ($p < 0.05$), suggesting that CsV could enhance the tube formation ability of HUVECs.

3.2 Effects of CsV on eNOS and vasodilation in mice

To verify the effects of CsV on eNOS and vasodilation in mice, male C57 BL/6 mice were administered with CsV intragastrically at 0, 50, 100, 150, and 200 mg/kg for 28 d. WB was used to detect eNOS protein expression, as shown in Figs. 3A and 3B. eNOS expression increased with the increase of CsV concentration ($p < 0.05$). The amount of cell NO release was detected as shown in Fig. 3E, and the amount of NO released also increased with the increase of CsV concentration ($p < 0.05$). We subsequently selected 200 mg/kg CsV to gavage the male C57 BL/6 mice and detected the expressions of eNOS protein on day 0, 7, 14, 21, and 28 d, using WB. The results were presented in Figs. 3C-3D, the expression levels of eNOS increased with the increase of CsV treatment time ($p < 0.05$), The cell NO release was detected as shown in Fig. 3F, and the NO release also increased with the increase of CsV treatment time ($p < 0.05$). According to the described experimental results, the optimal concentration (200 mg/kg) and optimal time (28 d) were selected for CsV intragastric administration of male C57 BL/6 mice and the aorta of mice were collected. RT-qPCR was used to detect the expression of eNOS mRNA (Fig. 4A) and the results showed that the expression of eNOS after CsV treatment was markedly higher than that of the control group ($p < 0.05$). WB detection was conducted to determine the protein expression of total eNOS and its phosphorylation sites. The results were shown in Figs. 4B and 4C. After CsV treatment the protein expressions of total eNOS and its phosphorylation sites were markedly elevated compared with the control group ($p < 0.05$). Further comparison of the protein expression levels of eNOS phosphorylation sites Ser1177, Ser633, and Thr495 and total eNOS indicated no statistical significance (Fig. 4D), suggesting that the increase of total eNOS protein content in mouse aortic endothelial cells resulted in the increase of corresponding phosphorylation site protein content.

Acetylcholine-mediated vasodilation was an important indicator of vascular endothelial activity. The functional status of endothelium-dependent vasodilation was closely related to endothelial integrity and ROS levels, especially the function status of eNOS. Therefore, we investigated the effect of CsV on acetylcholine-mediated vasodilation. The role of ACh-mediated endothelial cell-dependent vasodilation in NE-induced aortic contraction was investigated in control and CsV groups. The aorta of mice which were administered

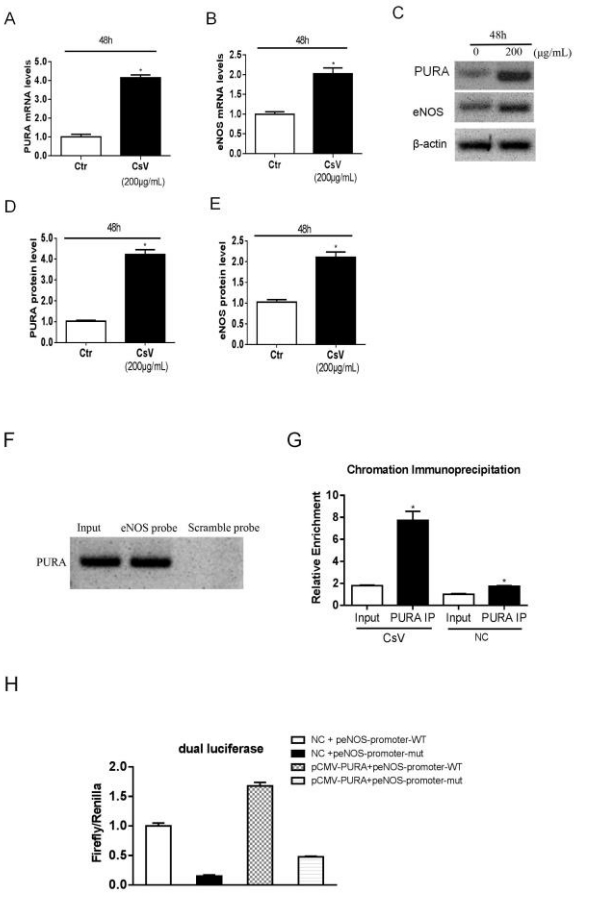

Fig. 6 Verification of PURA binding to eNOS promoting eNOS transcription

with the optimal concentration and time intragastrically was taken for vasodilation function detection. The vasodilation test was performed using acetylcholine at a concentration of 10^{-8}-$10^{-5.5}$ M (Fig. 4E). The percentage of vasodilation in CsV group was higher than that in control group ($p < 0.05$). Results of Ach concentration (EC_{50}) that produced 50% vasolatation in aorta were shown in Fig. 4F. EC_{50} of mice in CsV group was lower than that in control group ($n = 5$, $p < 0.05$). PWV measurement has been considered as a gold standard method for assessing atherosclerosis and has been well validated as a powerful predictor of adverse cardiovascular outcomes in a large population. Aortic arch pulse wave velocity was measured by B-ultrasound in male C57 BL/6 mice after optimal concentration and time of intragastric administration to reflect aortic stiffness. Ultrasonic imaging was firstly used to measure the root diameter of aortic annulus, sinus of valsalva and sinotubular junction (Fig. 4G, left). The results were shown as follows (Figs. 4H-4J). In the aortic annulus measurement, no significant statistical difference was revealed between the results of the control group and the CsV group. In sinus of valsalva measurement, the root diameter of CsV group was larger than that of control group, and the difference was statistically significant ($n = 5$, $p < 0.005$). In sinotubular junction measurement, the root diameter of CsV group was larger than that of the control group, and the difference was statistically significant ($n = 5$, $p < 0.005$). A representative B-ultrasound view of aortic arch distance was shown in Fig. 4G (right). PWV results of the two groups of mice were calculated according to PWV = D1/[T2-T1 (cm/s)] (Fig. 4K). PWV of CsV group was lower than that of control group, and the difference was statistically significant ($n = 5$, $p < 0.05$).

3.3 Prediction and screening of eNOS upstream transcription factors

The molecular structure of CsV was exported from the Pubchem database, and the action target of CsV was predicted and sorted from the SwissTargetPrediction website (Fig. 5B) including Ptafr, Hsd11b1, F2, Hsd11b2, Ptpn1, PURA, and FEV. The eNOS promoter sequence was predicted through the NCBI website, and the upstream transcription factors that might bind to eNOS were predicted via the AnimalTFDB3.0 website. Meanwhile, we performed eNOS transcription factor mass spectrometry analysis on BAECs cells treated with 100 μM CsV for 24 h (Fig. 5A). The results of mass spectrometry analysis, CsV target prediction and eNOS upstream transcription factor prediction were overlapped with PURA and FEV. The binding effect of CsV and PURA was analyzed using AutoDock software. As shown in Fig. 5D, CsV and PURA had hydrogen bonding effect, while FEV did not find hydrogen bonding effect with CsV. Therefore, PURA was selected as the eNOS candidate transcription factor, and PURA binding to the eNOS promoter was shown in Fig. 5C.

3.4 RT-qPCR and WB verification of the mRNA and protein expression levels of PURA in BAECs cells after CsV treatment

BAECs were treated with 100 μM CsV for 24 h, and total cell RNA was extracted. After reverse transcription, RT-qPCR was performed to detect the mRNA expression levels of the mentioned candidate transcription factors. According to the verification results of RT-qPCR, the mRNA expression levels of PURA and eNOS in BAECs cells treated with CsV were higher than those in the control group (Figs. 6A and 6B). The difference was statistically significant ($p < 0.05$). WB was further employed to verify the expression differences of PURA and eNOS proteins in BAECs cells treated with the optimal time and concentration of CsV. The results were shown in Fig. 6C. The WB results indicated that the protein expression levels of PURA and eNOS in BAECs treated with CsV were higher than those in the control group (Figs. 6D-6E). The difference was statistically significant ($p < 0.05$).

3.5 Pull down assay verifies the binding of PURA to eNOS promoter sequence

The Pull down experiment results showed that PURA might bind to eNOS promoter, and the expression of PURA was up-regulated after CsV addition ($p < 0.05$, Fig. 6F).

3.6 Chromatin immunoprecipitation assay (ChIP) verifies the binding of PURA to eNOS promoter sequence

To further verify the transcriptional regulation of PURA on eNOS gene, ChIP experiment was first performed, to

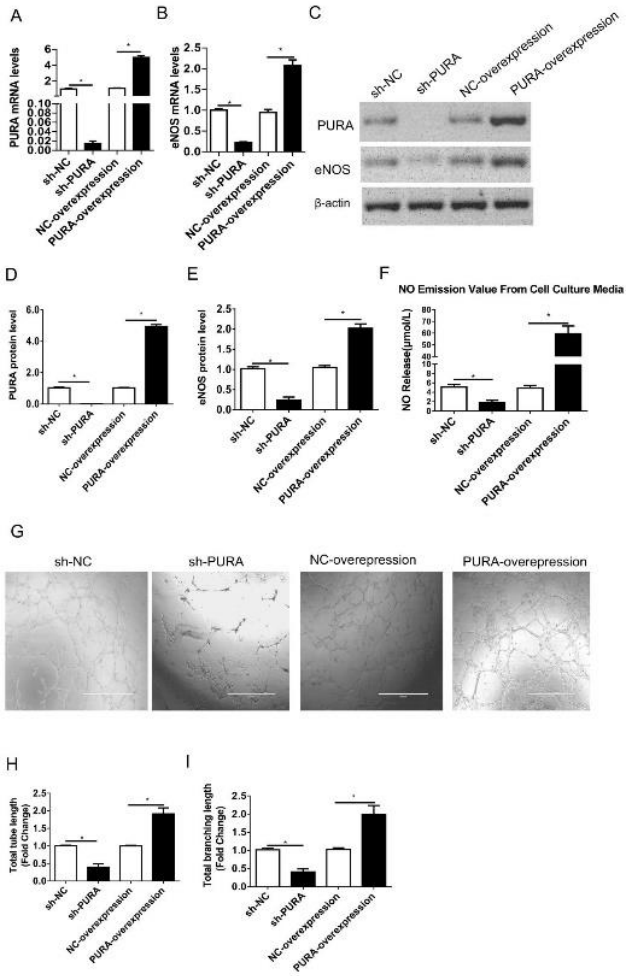

Fig. 7 Effects of PURA knockout or overexpression on eNOS expression and endothelial functions in BAEC cells

clarify whether PURA protein could bind to the promoter sequence of eNOS gene. The promoter sequence of eNOS gene was determined through retrieval of the NCBI website, and then the possible binding site of PURA on the eNOS promoter sequence was predicted as procedures of Animal TFDB3.0 website. The RT-qPCR detection results followed by ChIP assays indicated that PURA might bind to the eNOS promoter, and the expression of PURA was upregulated after the addition of CsV ($p < 0.05$, Fig. 6G).

3.7 Dual luciferase gene reporter assays

To perform dual luciferase gene reporter assays, the following plasmids were constructed according to the predicted sites on the eNOS gene promoter that might bind to the PURA protein on the AnimalTFDB3.0 website: peNOS-promoter-WT plasmid and peNOS-promoter-mut plasmid. NC+peNOS-promoter-WT, NC+peNOS-promoter-mut, pCMV-PURA+peNOS-promoter-WT, and pCMV-PURA+peNOS-promoter-mut were co-transfected into HEK293 cells using transfection reagents, respectively, and each group of cells was transfected with renilla luciferase plasmid for calibration. The detection results of different groups of luciferase activities after transfection were shown in Fig. 6F. The fluorescence activity of peNOS-promoter-WT group was significantly higher than that of NC+peNOS-promoter-mut group ($p < 0.05$), and the fluorescence activity of pCMV-PURA+peNOS-promoter-mut group was higher than that of NC+peNOS-promoter-mut group ($p < 0.05$). The fluorescence activity of pCMV-PURA+peNOS-promoter-WT group was significantly higher than the remaining three groups ($p < 0.05$). The results indicated that PURA could bind to the eNOS promoter sequence and promote the transcription of eNOS gene.

3.8 Effects of PURA knockout or overexpression on eNOS expression and endothelial functions in BAECs

The mRNA and protein expressions of PURA and eNOS were detected by RT-qPCR and WB, to verify the changes of endothelial function after knockout or overexpression of PURA gene in BAECs. The experiment grouping included as follows: sh-PURA group, sh-NC group, PURA-overexpression group, and NC-over-expression group. The experimental results were presented in Figs. 7A and 7B that the mRNA expressions of PURA and eNOS in BAECs were detected by RT-qPCR. After PURA was silenced, the mRNA expressions of PURA and eNOS were significantly decreased compared with the control group, with statistical significance ($p < 0.05$). After overexpression of PURA, the mRNA expressions of PURA and eNOS were significantly increased compared with the control group, with statistical significance ($p < 0.05$). As shown in Figs. 7C-7E, the protein expression levels of PURA and eNOS in BAECs were detected by WB. Following PURA silence, the protein expressions of PURA and eNOS were significantly decreased compared with the control group, with statistical significance ($p < 0.05$). As shown in Fig. 7F, the NO release in BAECs was detected. Following PURA silence, the NO release in BAECs was significantly lower than that of the control group ($p < 0.05$), after PURA overexpression, the NO release in BAECs increased significantly compared with the control group and the difference was statistically significant ($p < 0.05$). As shown in Fig. 7G-I, tube formation experiment was conducted to detect the tube formation capability of HUVECs. After PURA silencing, the total tubule length and total branch length of HUVECs decreased compared with the control group and the difference was statistically significant ($p < 0.05$). After overexpression of PURA, the total tubule length and total branch length of HUVECs were slightly increased compared with the control group, which was statistically significant ($p < 0.05$). The above experimental results indicated that PURA could improve the endothelial function of BAECs and enhance the tube formation ability of HUVECs by upregulating the expression of eNOS.

3.9 Effects of CsV on eNOS expression and endothelial function in BAECs with PURA knockout or overexpression

The previously described results indicated that PURA could change the endothelial function of cells by up-regulating the expression of eNOS. To further detect the effects of CsV on eNOS expression and endothelial function

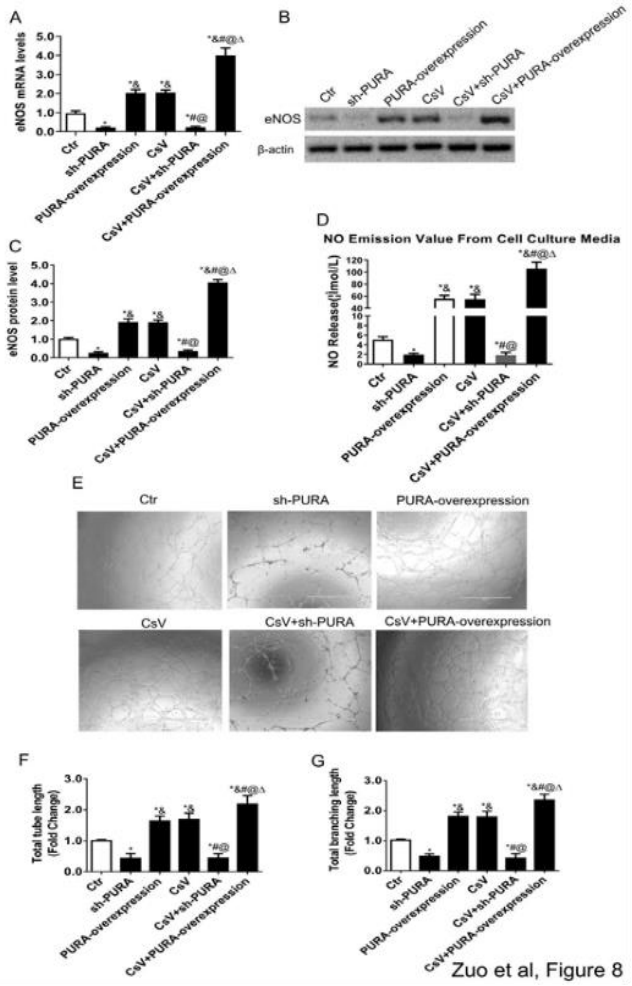

Fig. 8 Effects of CsV on eNOS expression and endothelial function in BAEC cells with PURA knockout or overexpression

function in BAECs with PURA knockout or overexpression, the optimal concentration (100 μM) and best time (24 h) of CsV treatment on BAECs following knockout or over-expression of PURA gene. The experiment was divided into six groups: control group, CsV group, sh-PURA group, PURA-overexpression group, CsV+sh-PURA group, and CsV+PURA-overexpression group. The experimental results were presented in Fig. 8A that the mRNA expressions of eNOS in BAECs were detected by RT-qPCR. Compared with the CsV+sh-PURA group, the mRNA expression of eNOS in the sh-PURA group had no significant change, and was lower than the other four groups ($p < 0.05$). The mRNA expression of eNOS in the PURA-overexpression group was higher than that in the control group ($p < 0.05$). However, after CsV treatment, the mRNA expression of eNOS in the CsV+PURA-over-expression group was higher than that in the other five groups ($p < 0.05$). The protein expression of eNOS in BAECs was detected by WB, as shown in Fig. 8B-C. Compared with the CsV+sh-PURA group, the protein expression of eNOS in the sh-PURA group had no significant change, and was lower than the other four groups ($p < 0.05$). The protein expression of eNOS in the PURA-overexpression group was higher than that in the control group ($p < 0.05$). However, after CsV treatment, the protein expression of eNOS in the CsV+PURA-overexpression group was higher than that in the other five groups ($p < 0.05$). The intracellular NO release from BAECs was detected, as shown in Fig. 8D. Compared with CsV+sh-PURA group, sh-PURA group had no significant change in NO release from cells, and was lower than the other four groups ($p < 0.05$). The amount of NO release from cells in the PURA-overexpression group was higher than that in the control group ($p < 0.05$). However after CsV treatment, the cell NO release in the CsV+PURA-overexpression group was higher than that in the other five groups ($p < 0.05$).

As shown in Figs. 8E-8G, tube formation experiment was conducted to detect the tube formation capability of HUVECs. Compared with the CsV+sh-PURA group, the total tubule length and total branch length of HUVECs in the sh-PURA group had no significant change, and were lower than those in the other four groups ($p < 0.05$). The total tubule length and total branch length of HUVECs in the PURA-overexpression group were longer than the control group ($p < 0.05$). After CsV treatment, the total tubule length and total branch length of HUVECs in CsV+PURA-overexpression group were longer than those in the other five groups ($p < 0.05$). Taken together, effects of CsV on vascular endothelial function and eNOS were weakened following PURA gene silence, whereas overexpression of PURA gene could enhance the effect of CsV upregulating eNOS expression. PURA/eNOS pathway might be the target of CsV regulation of eNOS expression and vasodilation functions.

3.10 CsV improves mRNA and protein expressions of PURA and eNOS in mice

To determine the effects of CsV on the expression of PURA and eNOS in animals, the optimal concentration (200 mg/kg) and optimal time (28 d) were selected for CsV intragastric administration of male C57 BL/6 mice and the aorta of mice were collected. The mRNA expressions ofPURA and eNOS were detected by RT-qPCR as shown in Figs. 9A and 9B. The mRNA expressions of PURA and eNOS were higher than the control group with statistical significance ($p < 0.05$). The protein expressions of PURA and eNOS were detected by WB as shown in Figs. 9C-9E. After CsV administration, the protein expressions of PURA and eNOS were significantly increased compared with the control group, and the difference was statistically significant ($p < 0.05$).

3.11 Effects of PURA knockout or overexpression on eNOS expression and endothelial functions in mice

According to silence or overexpression of PURA gene, male C57 BL/6 mice were grouped into sh-PURA group, sh-NC group, PURA-overexpression group, and NC-over-expression group. Aortic endothelial cells were taken from the mice, and the mRNA and protein expression levels of PURA and eNOS, NO release, vasodilation function and degrees of atherosclerosis were detected to determine the effects of PURA gene on eNOS expression and endothelial

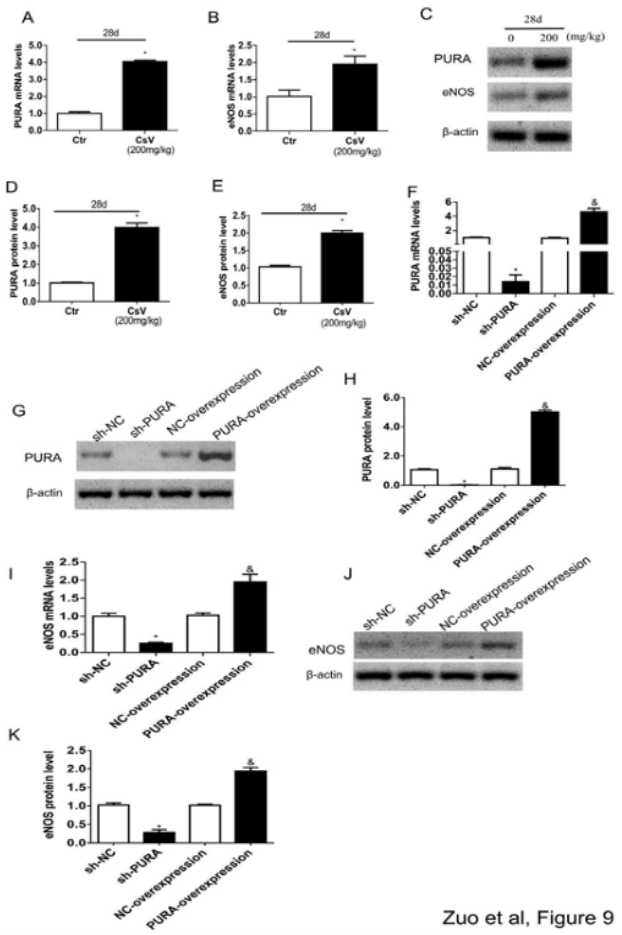

Fig. 9 CsV improved mRNA and protein expression of PURA and eNOS in mice

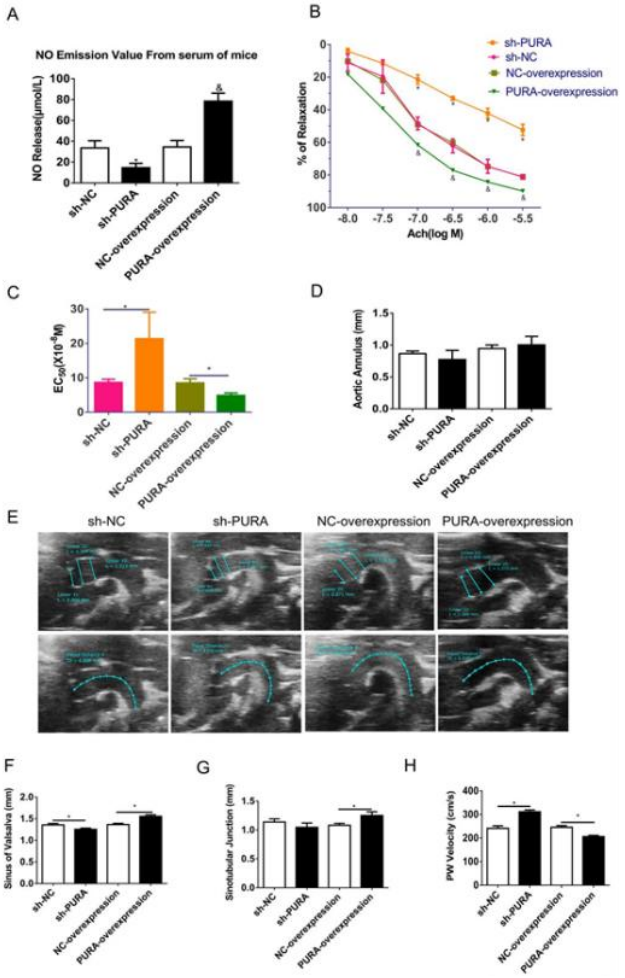

Fig. 10 Effects of PURA knockout or overexpression on eNOS expression and endothelial functions in mice

function of mice. The experimental results were presented by RT-qPCR detection as shown in Figs. 9F and 9I. The mRNA expressions of PURA and eNOS in the sh-PURA group were lower than those in the sh-NC group ($p < 0.05$), whereas the mRNA expressions of PURA and eNOS in the PURA-overexpression group were higher than those in the NC-overexpression group ($p < 0.05$), WB detection were shown in Figs. 9G-9H, 9J-9K. The protein expressions of PURA and eNOS in the sh-PURA group were lower than those in the sh-NC group ($p < 0.05$), and those in the PURA-overexpression group were higher compared with the NC-overexpression group ($p < 0.05$). The NO release of mouse aortic endothelial cells was detected and shown in Fig. 10A. The cell NO release in the sh-PURA group was lower than that in the sh-NC group ($p < 0.05$), and that of the PURA-overexpression group was higher than the NC-overexpression group ($p < 0.05$).

We further explored the effect of knockout or over-expression of PURA gene on acetylcholine-mediated vasodilation in mice. Vasodilation assays were performed using acetylcholine at the concentration of 10^{-8}-$10^{-5.5}$ M, as shown in Fig. 10B. The percentage of vasodilation in the sh-PURA group was lower than that in the sh-NC group ($p < 0.05$), while the percentage of vasodilation in the PURA-overexpression group was greater than that in the NC-overexpression group ($p < 0.05$). The Ach concentration (EC_{50}) results of 50% vasodilation in the aorta were shown in Fig. 10C. The concentration of Ach for 50% vasodilation in the aorta of mice in the sh-PURA group was higher than that in the sh-NC group ($p < 0.05$), whereas the concentration of Ach for 50% vasodilation in the aorta of mice in the PURA-overexpression group was lower than that in the NC-overexpression group ($p < 0.05$). Aortic arch pulse wave velocity was measured by B-mode ultrasound in male C57 BL/6 mice after PURA gene was knocked out or overexpressed to reflect aortic stiffness. Ultrasonic imaging was firstly used to measure the root diameter of aortic annulus, sinus of valsalva and sinotubular junction (upper Fig. 10E). The results were exhibited as follows (Fig. 10D, F, and G), in the aortic annulus measurement, no statistical difference was revealed among sh-PURA group, sh-NC group, PURA-overexpression group and NC-overexpression group. In the sinus of valsalva measurement, the length of sinus of valsalva in the sh-PURA group was shorter than that in the sh-NC group ($p < 0.005$), and sinus of Valsalva length in the PURA-overexpression group was longer than that in the NC-overexpression group ($p < 0.005$), In the measurement of sinotubular junction, there was no statistical difference in the length of sinotubular junction between sh-PURA group and sh-NC group. The length of sinotubular junction in PURA-overexpression group was

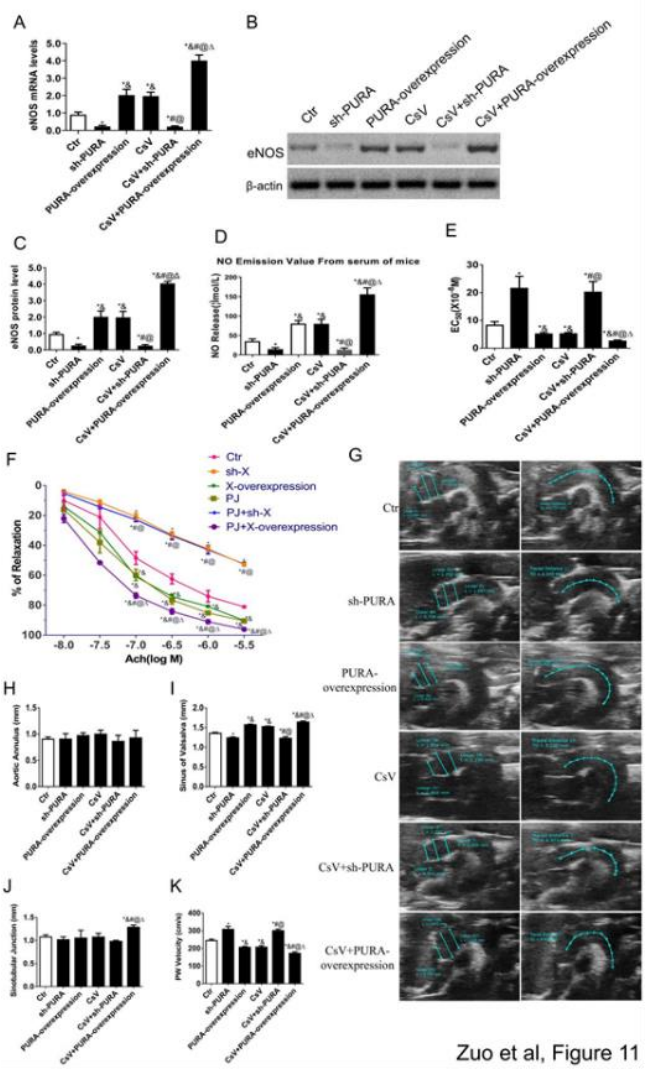

Fig. 11 Effects of CsV on eNOS expression and endothelial function in mice with PURA knockout or overexpression

longer than that in NC-overexpression group ($p < 0.005$). A representative B-ultrasound view of the aortic arch distance was shown in Fig. 10E (lower). The PWV results of the four groups of mice were calculated according to PWV = D1/[T2 - T1 (cm/s)] (Fig. 10H). The PWV in sh-PURA group was greater than sh-NC group ($p < 0.005$) but those in PURA-overexpression smaller than the NC-over-expression group ($p < 0.005$). The above results indicated that PURA could upregulate the expression of eNOS in mice, increase NO release from mouse aortic endothelial cells, fortify vasodilation function, and alleviate the degree of arteriosclerosis.

3.12 Effects of CsV on eNOS expression and endothelial function in mice with PURA knockout or overexpression

To further detect the effects of CsV on eNOS expression, endothelial function, vasodilation function and degree of arteriosclerosis in mice with PURA gene knockout or overexpression, male C57 BL/6 mice were intragastrically administrated with CsV at the optimal concentration (200 mg/kg) and time (28 d), and the aorta of mice were subsequently obtained. Based on PURA overexpression or silence and CsV intervention, the experiment was divided into six groups: control group, CsV group, sh-PURA group, PURA-overexpression group, CsV+sh-PURA group, and CsV+PURA-overexpression group. The experimental results were presented in Fig. 11A that the mRNA expressions of eNOS in endothelial cells of mouse aorta were detected by RT-qPCR. Compared with the CsV+sh-PURA group, the mRNA expression of eNOS in the sh-PURA group had no significant change, and was lower than the other four groups ($p < 0.05$), whereas the mRNA expression of eNOS in the PURA-overexpression group was higher than that in the control group ($p < 0.05$). However, after CsV treatment, the mRNA expression of eNOS in the CsV+PURA-overexpression group was higher than that in the other five groups ($p < 0.05$). The protein expression of eNOS in endothelial cells of mouse aorta was detected by WB, as shown in Figs. 11B and 11C. Compared with the CsV+sh-PURA group, the protein expression of eNOS in the sh-PURA group had no significant change, and was lower than the other four groups ($p < 0.05$), The protein expression of eNOS in the PURA-overexpression group was higher than that in the control group ($p < 0.05$). However, after CsV treatment, the protein expression of eNOS in the CsV+PURA-overexpression group was higher than that in the other five groups ($p < 0.05$). The NO release of mouse aortic endothelial cells was detected and shown in Fig. 11D. Compared with CsV+sh-PURA group, sh-PURA group had no significant change in cell NO release, and was lower than the other four groups ($p < 0.05$). The cell NO release in the PURA-overexpression group was higher than that in the control group ($p < 0.05$). However, after CsV treatment, the cell NO release in the CsV+PURA-over-expression group was higher than that in the other five groups ($p < 0.05$). Vasodilation assays were performed using acetylcholine at the concentration of 10^{-7}-$10^{-5.5}$ M, as shown in Fig. 11F. Compared with CsV+sh-PURA group, sh-PURA group had no significant change in percentage of vasodilation, which was lower than the other four groups ($p < 0.05$). The percentage of vasodilation in the PURA-overexpression group was higher than that in the control group ($p < 0.05$). However, after CsV treatment, the percentage of vasodilation in the CsV+PURA-over-expression group was higher than that in the other five groups ($p < 0.05$). The Ach concentration (EC_{50}) results of 50% vasodilation in the aorta were shown in Fig. 11E. Compared with CsV+sh-PURA group, sh-PURA group had no significant change in EC_{50}, which was higher than the control ($p < 0.05$).

EC_{50} in the PURA-overexpression group was lower than that in the control group ($p < 0.05$). However, after CsV treatment, EC_{50} in the CsV+PURA-overexpression group was lower than that in the other five groups ($p < 0.05$).

B ultrasonic detection was performed to determine the mouse aortic arch pulse wave velocity to identify aortic stiffness (Fig. 11G). Ultrasonic imaging was conducted to measure the root diameter of aortic annulus, sinus of valsalva and sinotubular junction (Fig. 11G, left). In the measurement of aortic annulus (Fig. 11H), there was no

statistical difference between the control group, CsV group, sh-PURA group, PURA-overexpression group, CsV+sh-PURA group, and CsV+PURA-overexpression group, In the measurement of sinus of valsalva (Fig. 11I), there was no statistical difference between the sh-PURA group and the CsV+sh-PURA group, and all were lower than the other four groups ($p < 0.05$). The root diameter of sinus of valsalva in the PURA-overexpression group was longer than that in the control group ($p < 0.05$), while the root diameter of the sinus of valsalva in the CsV+PURA-overexpression group after CsV treatment was longer than the other five groups ($p < 0.05$). In the measurement of sinotubular junction (Fig. 11J), there was no statistical difference in the root diameter length among the control group, CsV group, SH-Pura group, Pura-Overexpression group, and CsV+ SH-Pura group whereas that of CsV+ PURa-overexpression group was longer than the rest five groups ($p < 0.05$). A representative B-ultrasound view of aortic arch distance was presented in Fig. 11G (right). PWV results of the six groups of mice were presented (Fig. 11K). There was no statistical difference between the sh-PURA group and the CsV+sh-PURa group, and both of them were greater than the other four groups ($p < 0.05$). PWV in the PURA-overexpression group was lower than that in the control group ($p < 0.05$). However, after CsV treatment, PWV in the CsV+PURA-overexpression group was lower than that in the other five groups ($p < 0.05$). The previously described results were in agreement with those of BAECs assays. After PURA gene silencing in mice, the effects of CsV on vascular endothelial function and eNOS were weakened, while overexpression of PURA gene enhanced the effect of CsV on eNOS expression. Further in vivo verification indicated that CsV might improve vascular endothelial functions through PURA/eNOS pathway.

4. Discussion

Cardiovascular disease is a common disease that seriously threatens the health of human beings, especially the middle-aged and elderly people above 50 years of age.

Even if modern medical treatment and inspection methods are relatively advanced, over 50% of patients may lose their lives unexpectedly or lose the ability to take care of themselves. The number of people lost lives due to cardiovascular disease in the world is as high as 15 million annually. Vascular endothelial cells, have a series of complex physiological functions including regulation of vasomotor and maintenance of stable hemorheology. It effectively guarantees the normal physiological function of the circulatory system (Wei *et al*. 2020). Endothelial cell dysfunction can initiate or promote the pathogenesis of various cardiovascular diseases (Zong *et al*. 2015). Endothelial cell dysfunction is initially characterized by altered NO bioactivity, downregulation of eNOS activity, and reduced endogenous NO production. Consequently, and endothelial-dependent vasodilation is impaired accordingly (Nicoll and Henein 2018). The PURA gene encodes a protein called PURα that consists of a DNA-binding domain, a glycine rich N-terminal domain, and a glutamine-glutamine rich C-terminal domain (Cinquina *et al*. 2021). It is widely found in various organisms and is highly conserved during evolution. Meanwhile, it involves in initiating DNA replication, transcriptional regulation and mRNA translation. The C-terminus of PURα protein is of vital significance in maintaining the stability of linear DNA. As a transcriptional activator, PURα binds to specific single-stranded DNA, affects the initiation of DNA replication, and promotes the transcription of specific genes (Bae *et al*. 2013), including promotion of the transcription of genes encoding TNF-α, myelin basic protein, β-integrin, placental prolactin, TGFβ-1, neuron-specific FE65 protein and PDGF-A protein (Zhang *et al*. 2012). Pura-related developmental disorders have also been found to be associated with congenital cardiovascular disease in recent studies (Reuter *et al*. 2020, Hou *et al*. 2021, Jiao *et al*. 2021, Liu *et al*. 2021, Moradi *et al*. 2021).

CsV is oleanolic acid type ginsenoside, which has anti-inflammatory, antiviral and immunomodulatory effects (Wang *et al*. 2016). Previous studies have reported its protection effect on the cardiovascular vessels (Cao *et al*. 2017) but its mechanisms remain unclear. This study revealed that CsV treated BAECs in vitro and mouse aortic endothelial cells in vivo improved the mRNA expression and protein expression of eNOS, enhanced the tube formation ability of HUVECs, increased the NO release of mouse aortic endothelial cells, and minimized the degree of aortic stiffness in mice. These data obtained suggested that CsV could improve endothelial cell function and endothelium dependent vasodilation by upregulating eNOS expression. To further understand the role of eNOS in the regulation of vascular endothelial function following CsV administration, and to clarify the molecular mechanism of CsV action, this study further explored the upstream mechanism of eNOS by means of prediction of transcription factors, network pharmacology analysis, and molecular docking. It has been identified that PURA might act as a transcription factor of eNOS, affect the transcription and expression of eNOS, and participate in the regulation of eNOS via CsV stimulus. Meanwhile, PURA could bind to eNOS promoter and promote eNOS transcription by protein spectrum analysis, ChIP assays and double luciferase assays. Knockdown or overexpression of PURA gene could upregulate the expression of eNOS, increase NO release of mouse aortic endothelial cells, and improve endothelial cell functions, Following CsV intervention in cells and mice with knockdown or overexpression of PURA gene, the results revealed that CsV could upregulate eNOS expression, improve endothelial cell functions, and alleviate arterial stiffness under the condition of PURA overexpression or normal expression. However, the effect of CsV was not obvious under the condition of PURA silencing, and there was no statistical difference with the negative control group. The previously described results demonstrated that CsV could promote eNOS transcription and improve endothelial cell functions by upregulating PURA expression.

5. Conclusions

CsV could promote NO release from endothelial cells

by upregulating the expression of PURA/eNOS pathway, improve endothelial cell functions, enhance vasodilation capability, and alleviate vessel stiffness. The present study plays a role in offering a theoretical basis for the development and application of CsV in vascular function improvement, and it also provides a more comprehensive understanding of the pharmacodynamics of CsV.

Acknowledgement

This work was supported by Chongqing Postdoctoral Innovative Talent Support Program (CQBX2021001) and the Special Project for Performance Incentive and Guidance of Scientific Research Institutions in Chongqing (cstc2021 jxjl130020, cstc2021jxjl130002).

References

Adamian, A., Safari, K.H., Sheikholeslami, M., Habibi, M., Al-Furjan, M. and Chen, G. (2020), "Critical temperature and frequency characteristics of gpls-reinforced composite doubly curved panel", *Appl. Sci.*, **10**(9), 3251. https://doi.org/10.3390/app10093251.

Bae, C.H., Kim, D.S., Jun, Y.L., Kwon, S., Park, H.J., Hahm, D.H., Lee, H. and Kim, S.T. (2013), "Proteomic analysis of the effect of acupuncture on the suppression of kainic acid-induced neuronal destruction in mouse hippocampus", *Evidence Based Complement. Altern. Med.*, **2013**, 436315. https://doi.org/10.1155/2013/436315.

Bai, Y., Alzahrani, B., Baharom, S. and Habibi, M. (2020), "Semi-numerical simulation for vibrational responses of the viscoelastic imperfect annular system with honeycomb core under residual pressure", *Eng. Comput.*, 1-26. https://doi.org/10.1007/s00366-020-01191-9

Boucher, J.L., Moali, C. and Tenu, J.P. (1999), "Nitric oxide biosynthesis, nitric oxide synthase inhibitors and arginase competition for L-arginine utilization", *Cell. Mole. Life Sci. CMLS.* **55**(8), 1015-1028. https://doi.org/10.1007/s000180050352.

Cao, Y., Gu, C., Zhao, F., Tang, Y., Cui, X., Shi, L., Xu, L. and Yin, L. (2017), "Therapeutic effects of Cyathula officinalis Kuan and its active fraction on acute blood stasis rat model and identification constituents by HPLC-QTOF/MS/MS", *Pharmacognosy Mag.*, **13**(52), 693-701. https://doi.org/10.4103/pm.pm_560_16.

Chen, F., Chen, J., Duan, R., Habibi, M. and Khadimallah, M.A. (2022), "Investigation on dynamic stability and aeroelastic characteristics of composite curved pipes with any yawed angle", *Compos. Struct.*, 115195. https://doi.org/10.1016/j.compstruct.2022.115195.

Cinquina, V., Ciaccio, C., Venturini, M., Masson, R., Ritelli, M. and Colombi, M. (2021), "Expanding the PURA syndrome phenotype: A child with the recurrent PURA p.(Phe233del) pathogenic variant showing similarities with cutis laxa", *Mol. Genet. Genomic Med.*, **9**(1), e1562. https://doi.org/10.1002/mgg3.1562.

Dai, Z., Jiang, Z., Zhang, L. and Habibi, M. (2021a), "Frequency characteristics and sensitivity analysis of a size-dependent laminated nanoshell", *Adv. Nano Res.*, **10**(2), 175-189. https://doi.org/10.12989/anr.2021.10.2.175.

Dai, Z., Zhang, L., Bolandi, S.Y. and Habibi, M. (2021b), "On the vibrations of the non-polynomial viscoelastic composite open-type shell under residual stresses", *Compos. Struct.*, 113599. https://doi.org/10.1016/j.compstruct.2021.113599.

Dong, Y., Gao, Y., Zhu, Q., Moradi, Z. and Safa, M. (2022), "TE-GDQE implementation to investigate the vibration of FG composite conical shells considering a frequency controller solid ring", *Eng. Anal. Bound. Elem.*, **138**, 95-107. https://doi.org/10.1016/j.enganabound.2022.01.017.

Ebrahimi, F., Hashemabadi, D., Habibi, M. and Safarpour, H. (2020), "Thermal buckling and forced vibration characteristics of a porous GNP reinforced nanocomposite cylindrical shell", *Microsyst. Technol.*, **26**(2), 461-473. https://doi.org/10.1007/s00542-019-04542-9.

Godo, S. and Shimokawa, H. (2017), "Endothelial functions", *Arterioscl. Throm. Vasc.*, **37**(9), e108-e114. https://doi.org/10.1161/ATVBAHA.117.309813.

Guo, Y., Mi, H. and Habibi, M. (2021), "Electromechanical energy absorption, resonance frequency, and low-velocity impact analysis of the piezoelectric doubly curved system", *Mech. Syst. Signal Pr.*, **157** 107723. https://doi.org/10.1016/j.ymssp.2021.107723.

Habibi, M., Darabi, R., Sa, J.C.D. and Reis, A. (2021), "An innovation in finite element simulation via crystal plasticity assessment of grain morphology effect on sheet metal formability", *Proceedings of the Institution of Mechanical Engineers, Part L: Journal of Materials: Design and Applications*, **235**(8), 1937-1951. https://doi.org/10.1177/14644207211024686.

Habibi, M., Hashemabadi, D. and Safarpour, H. (2019a), "Vibration analysis of a high-speed rotating GPLRC nano-structure coupled with a piezoelectric actuator", *Eur. Phys. J. Plus*, **134**(6), 307. https://doi.org/10.1140/epjp/i2019-12742-7.

Habibi, M., Taghdir, A. and Safarpour, H. (2019b), "Stability analysis of an electrically cylindrical nanoshell reinforced with graphene nanoplatelets", *Compos. Part B Eng.*, **175**, 107125. https://doi.org/10.1016/j.compositesb.2019.107125.

Hou, F., Wu, S., Moradi, Z. and Shafiei, N. (2021a), "The computational modeling for the static analysis of axially functionally graded micro-cylindrical imperfect beam applying the computer simulation", *Eng. Comput.*, 1-19. https://doi.org/10.1007/s00366-021-01456-x.

Huang, X., Hao, H., Oslub, K., Habibi, M. and Tounsi, A. (2021a), "Dynamic stability/instability simulation of the rotary size-dependent functionally graded microsystem", *Eng. Comput.*, 1-17. https://doi.org/10.1007/s00366-021-01399-3.

Huang, X., Zhang, Y., Moradi, Z. and Shafiei, N. (2021b), "Computer simulation via a couple of homotopy perturbation methods and the generalized differential quadrature method for nonlinear vibration of functionally graded non-uniform micro-tube", *Eng. Comput.*, 1-18. https://doi.org/10.1007/s00366-021-01395-7.

Huang, X., Zhu, Y., Vafaei, P., Moradi, Z. and Davoudi, M. (2021c), "An iterative simulation algorithm for large oscillation of the applicable 2D-electrical system on a complex nonlinear substrate", *Eng. Comput.*, 1-13. https://doi.org/10.1007/s00366-021-01320-y.

Huang, X., Zhu, Y., Vafaei, P., Moradi, Z. and Davoudi, M. (2021d), "An iterative simulation algorithm for large oscillation of the applicable 2D-electrical system on a complex nonlinear substrate", *Eng. Comput.*, 1-13. https://doi.org/10.1007/s00366-021-01320-y.

Jiao, J., Ghoreishi, S.M., Moradi, Z. and Oslub, K. (2021), "Coupled particle swarm optimization method with genetic algorithm for the static–dynamic performance of the magneto-electro-elastic nanosystem", *Eng. Comput.*, 1-15. https://doi.org/10.1007/s00366-021-01391-x.

Li, J., Tang, F. and Habibi, M. (2020a), "Bi-directional thermal buckling and resonance frequency characteristics of a GNP-reinforced composite nanostructure", *Eng. Comput.*, 1-22.

https://doi.org/10.1007/s00366-020-01110-y.
Li, Y., Li, S., Guo, K., Fang, X. and Habibi, M. (2020b), "On the modeling of bending responses of graphene-reinforced higher order annular plate via two-dimensional continuum mechanics approach", *Eng. Comput.*, 1-22. https://doi.org/10.1007/s00366-020-01166-w.
Liu, Z., Su, S., Xi, D. and Habibi, M. (2020a), "Vibrational responses of a MHC viscoelastic thick annular plate in thermal environment using GDQ method", *Mech. Based Des. Struct.*, 1-26. https://doi.org/10.1080/15397734.2020.1784201.
Liu, Z., Wu, X., Yu, M. and Habibi, M. (2020b), "Large-amplitude dynamical behavior of multilayer graphene platelets reinforced nanocomposite annular plate under thermo-mechanical loadings", *Mech. Based Des. Struct.*, 1-25. https://doi.org/10.1080/15397734.2020.1815544.
Liu, Y., Wang, W., He, T., Moradi, Z. and Larco Benítez, M.A. (2021a), "On the modelling of the vibration behaviors via discrete singular convolution method for a high-order sector annular system", *Eng. Comput.*, 1-23. https://doi.org/10.1007/s00366-021-01454-z.
Luo, J., Song, J., Moradi, Z., Safa, M. and Khadimallah, M.A. (2022), "Effect of simultaneous compressive and inertia loads on the bifurcation stability of shear deformable functionally graded annular fabrications reinforced with graphenes", *Eur. J. Mech. A Solids*, 104581. https://doi.org/10.1016/j.euromechsol.2022.104581.
Ma, L., Liu, X. and Moradi, Z. (2021), "On the chaotic behavior of graphene-reinforced annular systems under harmonic excitation", *Eng. Comput.*, 1-25. https://doi.org/10.1007/s00366-020-01210-9.
Moradi, Z., Davoudi, M., Ebrahimi, F. and Ehyaei, A.F. (2021), "Intelligent wave dispersion control of an inhomogeneous micro-shell using a proportional-derivative smart controller", *Wave Random Complex.*, 1-24. https://doi.org/10.1080/17455030.2021.1926572.
Nicoll, R. and Henein, M.Y. (2018), "Caloric restriction and its effect on blood pressure, heart rate variability and arterial stiffness and dilatation: A review of the evidence", *Int. J. Mol. Sci.*, **19**(3), 751. https://doi.org/10.3390/ijms19030751.
Reuter, M.S., Chaturvedi, R.R., Liston, E., Manshaei, R., Aul, R.B., Bowdin, S., Cohn, I., Curtis, M., Dhir, P., Hayeems, R.Z., Hosseini, S.M., Khan, R., Ly, L.G., Marshall, C.R., Mertens, L., Okello, J.B.A., Pereira, S.L., Raajkumar, A., Seed, M., Thiruvahindrapuram, B., Scherer, S.W., Kim, R.H. and Jobling, R.K. (2020), "The cardiac genome clinic: Implementing genome sequencing in pediatric heart disease", *Genet. Med.*, **22**(6), 1015-1024. https://doi.org/10.1038/s41436-020-0757-x.
Shao, Y., Zhao, Y., Gao, J. and Habibi, M. (2021), "Energy absorption of the strengthened viscoelastic multi-curved composite panel under friction force", *Arch. Civil Mech. Eng.*, **21**(4), 1-29. https://doi.org/10.1007/s43452-021-00279-3.
Tsutsui, M., Shimokawa, H., Otsuji, Y., Ueta, Y., Sasaguri, Y. and Yanagihara, N. (2009), "Nitric oxide synthases and cardiovascular diseases insights from genetically modified mice", *Circ. J.*, **73**(6), 986-993. https://doi.org/10.1253/circj.CJ-09-0208.
Vanhoutte, P.M., Shimokawa, H., Feletou, M. and Tang, E.H.C. (2017), "Endothelial dysfunction and vascular disease – a 30th anniversary update", *Acta Physiol.*, **219**(1), 22-96. https://doi.org/10.1111/apha.12646.
Wang, H.P., Zhang, Y.B., Yang, X.W., Yang, X.B., Xu, W., Xu, F., Cai, S.Q., Wang, Y.P., Xu, Y.H. and Zhang, L.X. (2016), "High-performance liquid chromatography with diode array detector and electrospray ionization ion trap time-of-flight tandem mass spectrometry to evaluate ginseng roots and rhizomes from different regions", *Molecules*, **21**(5), 603. https://doi.org/10.3390/molecules21050603.
Wei, A., Xiao, H., Xu, G., Yu, X., Guo, J., Jing, Z., Shi, S. and Song, Y. (2020), "Hyperoside protects human umbilical vein endothelial cells against anticardiolipin antibody-induced injury by activating autophagy", *Front. Pharmacol.*, **11**. https://doi.org/10.3389/fphar.2020.00762.
Wu, J. and Habibi, M. (2021), "Dynamic simulation of the ultra-fast-rotating sandwich cantilever disk via finite element and semi-numerical methods", *Eng. Comput.*, 1-17. https://doi.org/10.1007/s00366-021-01396-6.
Xu, W., Pan, G., Moradi, Z. and Shafiei, N. (2021), "Nonlinear forced vibration analysis of functionally graded non-uniform cylindrical microbeams applying the semi-analytical solution", *Compos. Struct.*, 114395. https://doi.org/10.1016/j.compstruct.2021.114395.
Yang, N., Moradi, Z., Khadimallah, M.A. and Arvin, H. (2022), "Application of the Chebyshev–Ritz route in determination of the dynamic instability region boundary for rotating nanocomposite beams reinforced with graphene platelet subjected to a temperature increment", *Eng. Anal. Bound. Elem.*, **139**, 169-179. https://doi.org/10.1016/j.enganabound.2022.03.013.
Yu, X., Maalla, A. and Moradi, Z. (2022), "Electroelastic high-order computational continuum strategy for critical voltage and frequency of piezoelectric NEMS via modified multi-physical couple stress theory", *Mech. Syst. Signal Pr.*, **165**, 108373. https://doi.org/10.1016/j.ymssp.2021.108373.
Zare, R., Najaafi, N., Habibi, M., Ebrahimi, F. and Safarpour, H. (2020), "Influence of imperfection on the smart control frequency characteristics of a cylindrical sensor-actuator GPLRC cylindrical shell using a proportional-derivative smart controller", *Smart Struct. Syst.*, **26**(4), 469-480. https://doi.org/10.12989/sss.2020.26.4.469.
Zhang, T., Zhang, H., Wang, Y. and McGown, L.B. (2012), "Capture and identification of proteins that bind to a GGA-rich sequence from the ERBB2 gene promoter region", *Anal. Bioanal. Chem.*, **404**(6), 1867-1876. https://doi.org/10.1007/s00216-012-6322-y.
Zhang, X., Shamsodin, M., Wang, H., NoormohammadiArani, O., Khan, A.M., Habibi, M. and Al-Furjan, M. (2020), "Dynamic information of the time-dependent tobullian biomolecular structure using a high-accuracy size-dependent theory", *J. Biomol. Struct. Dyn.*, 1-16. https://doi.org/10.1080/07391102.2020.1760939.
Zhang, Y., Wang, Z., Tazeddinova, D., Ebrahimi, F., Habibi, M. and Safarpour, H. (2021), "Enhancing active vibration control performances in a smart rotary sandwich thick nanostructure conveying viscous fluid flow by a PD controller", *Wave Random Complex.*, 1-24. https://doi.org/10.1080/17455030.2021.1948627.
Zhao, Y., Moradi, Z., Davoudi, M. and Zhuang, J. (2021), "Bending and stress responses of the hybrid axisymmetric system via state-space method and 3D-elasticity theory", *Eng. Comput.*, 1-23. https://doi.org/10.1007/s00366-020-01242-1.
Zhou, C., Zhao, Y., Zhang, J., Fang, Y. and Habibi, M. (2020), "Vibrational characteristics of multi-phase nanocomposite reinforced circular/annular system", *Adv. Nano Res.*, **9**(4), 295-307. https://doi.org/10.12989/anr.2020.9.4.295.
Zong, Y., Huang, Y., Chen, S., Zhu, M., Chen, Q., Feng, S., Sun, Y., Zhang, Q., Tang, C., Du, J. and Jin, H. (2015), "Downregulation of endogenous hydrogen sulfide pathway is involved in mitochondrion-related endothelial cell apoptosis induced by high salt", *Oxid. Med. Cell. Long.*, **2015**, 754670. https://doi.org/10.1155/2015/754670.